Kalman-Filter-Based Semi-Codeless Tracking of Weak Dual-Frequency GPS Signals

by Hee Jung, Mark L. Psiaki, and Steven P. Powell
Cornell University, Ithaca, N.Y. 14853-7501

BIOGRAPHY

Hee Jung is a Ph.D. candidate in Mechanical and Aerospace Engineering at Cornell University. She received her B.S. and M.S. in Astronomy from the Seoul National University in Korea and another M.S. in Aerospace Engineering from Texas A&M University. Her main research interests are GPS software receiver development and GPS applications, Kalman filter and estimation, orbit and attitude determination of satellites.

Mark L. Psiaki is an Associate Professor of Mechanical and Aerospace Engineering at Cornell University. He received a B.A. in Physics, and M.A. and Ph.D. degrees in Mechanical and Aerospace Engineering from Princeton University. His research interests are in the areas of estimation and filtering, spacecraft attitude and orbit determination, and GPS technology and applications.

Steven P. Powell is a Senior Engineer with the Space Plasma Physics Group in the Department of Electrical and Computer Engineering at Cornell University. He has been involved with the design, fabrication, and testing of several GPS receivers. He has M.S. and B.S. degress in Electrical Engineering from Cornell University.

ABSTRACT

Extended Kalman-Filter (EKF) based methods have been developed for semi-codeless tracking of the P(Y) code on weak dual-frequency GPS signals. Optimal Kalman filtering methods are essential to maintain lock with a semi-codeless approach during ionospheric scintillations, when deep power fades can occur. EKF-based semi-codeless techniques use maximum a posteriori estimation techniques to estimate the unknown W code that gets modulo-2 added to the P code in order to provide anti-spoofing protection. These tracking techniques take advantage of the known W-bit chip timing, whose chipping rate is approximately 500 KHz. They also use a posteriori cost functions that involve -log[cosh()] terms, which allow seamless transition between various W-bit decision techniques. The algorithm estimates the P(Y) carrier amplitudes, accounts for signal dynamics in the optimization process, and optimally couples its code and carrier tracking loops. The algorithm has been successfully tested with real data under normal signal strength conditions.

INTRODUCTION

Current dual-frequency GPS signals include the L1 carrier at 1575.42 MHz and the L2 carrier at 1227.6 MHz. The C/A code and the P code are modulated on L1, and only the P code is modulated on L2. When the anti-spoofing mode is on, an unknown W PRN code is modulo-2 added to the P code to generate the encrypted P(Y) code. The tracking of the P(Y) code on L2 by civilian users is hindered by the encryption.

L2 P(Y) signal tracking without knowledge of the encrypted code can be accomplished using either codeless or semi-codeless techniques. Codeless methods do not use any assumptions about the W code, and semi-codeless methods use the known chipping rate of the W code at about 500 kHz. The advantage of semi-codeless methods is that they can use a longer coherent summation interval, approximately 2μsec, before they must square or cross-correlate the signal. This longer interval increases the SNR, thus reducing the SNR loss due to squaring or due to cross-correlation.

Extended Kalman-Filter (EKF)/Smoother based methods are being developed for semi-codeless tracking of the P(Y) code on weak dual-frequency GPS signals. These are targeted for use in an off-line software receiver system that will be used for dual-frequency ionospheric scintillation monitoring. Optimal Kalman filtering/smoothing methods are essential to this application because a semi-codeless dual-frequency receiver is prone to lose lock due to the phase variations and amplitude fades that occur during ionospheric scintillations. Optimal tracking methods, especially those that employ non-causal smoothing, provide the highest possible degree of protection against loss of lock.

Woo (Ref. 1) summarized various conventional codeless and semi-codeless L2 carrier tracking methods. These include squaring, cross-correlation, P-code aided L2 squaring, and Z-tracking. He also introduced new methods such as a P-code aided L2 Costas loop, P-code aided L1 and L2 cross-correlation, soft decision Z-tracking, and a maximum a posteriori (MAP) method

Preprint from ION GPS/GNSS 2003

based partially on statistical estimation theory. His MAP method shows the best performance in P(Y) tracking in comparison to all other methods presented in Ref. 1, but it still requires a C/N_0 of at least 37 dB Hz on L2 to maintain an RMS phase error of 10 deg or less with a loop bandwidth of 10 Hz. Although Woo's MAP method is based on optimization techniques, it is not a full Kalman filter. It fails to consider the effects of variations in the carrier amplitudes, and it fails to incorporate a dynamics model to create a complete optimal estimation problem.

The current EKF based algorithm has several advantages over Woo's MAP method. First of all, it directly estimates the P(Y) carrier amplitudes on L1 and L2. Woo assumes constant P(Y) carrier amplitudes. Optimal estimation of the P(Y) carrier amplitudes allows the tracking algorithm to adjust for differential fade characteristic at the two carrier frequencies, which can occur during strong scintillations. If L1 fades, then the burden of estimating the W code bits falls to the L2 signal, and vice versa. In effect, this approach allows the carrier tracking to seamlessly transition between methods for dealing with the unknown W chips depending on the different ratios of the carrier amplitudes on the two frequencies. Second, signal dynamics model is explicitly included in the optimization process. Third, code and carrier tracking is optimally coupled in both the Kalman filter (applicable in real-time) and the non-causal smoother (for use off-line).

The remaining sections of this paper present the W code timing analysis (Section II), the signal dynamics and measurement models used to develop the algorithms (Section III), the EKF for P(Y) tracking on L2 (Section IV), experimental test results (Section V), and conclusions and planned future work.

II. W CODE TIMING ANALYSIS

The semi-codeless techniques use the known chip timing characteristics of the W code. W code timing analysis has been used to find the exact W code intervals to maximize the performance of the optimal semi-codeless tracking algorithm.

The duration of each unknown W code chip is known to be approximately 20 P code chips. US patents [2, 3] claim that the W-bit duration follows certain pattern and is not constant. They report that *M* W chips, each of length *A* P-code chips, are followed by *N* W chips, each of length *B* P-code chips. This pattern is then repeated ad infinitum. The duration of this repetition is reported to be $AM + BN = 4092$ where 4092 is the length of the X1A code, and this pattern is reported to be synchronous with the X1A code. Recall that the X1A code is one of 4 PRN codes that are used to construct the P code. The values of *A*, *M*, *B*, and *N* and the period of the repetition, $AM + BN = 4092/L$ where *L* is positive integer, have been estimated by applying the correlation techniques to L1 P(Y) data and by considering L1 P(Y) data from a high-gain antenna [4]. L has been found to be an integer greater than 1, but the patterns are still synchronous with the X1A code – there are *L* patterns of *A* times *M* plus *B* times *N* for each X1A code period. This estimated W-bit timing is used in the present tracking algorithm. Since the algorithm accumulates correlation over each W-bit interval, it is important to use the correct accumulation interval in order to maximize the signal-to-noise ratio in the accumulated data.

III. SIGNAL DYNAMICS AND MEASUREMENT MODELS

The EKF works with mathematical models at the signal dynamics and the accumulation measurements. The signal dynamics models describe the time evolution of important signal characteristics that need to get estimated. These include the carrier phase and code phase of P(Y) on L2 and the carrier amplitudes of P(Y) on L1 and L2. Measurement model describes the relationship between these signal quantities and accumulations of P(Y) on L1 and L2 over individual W-bit intervals.

A. Signal Model of Dual-Frequency RF Front End

The down-converted and sampled output signal of the dual-frequency RF front end that has been used in this work can be modeled as:

$$\begin{aligned} y(t_j) = {} & A_C(t_j)\,C[t_j-\tau_1(t_j)]D[t_j-\tau_1(t_j)]\cos[\omega_{\text{ifL1}}t_j+s_1\phi_1(t_j)] \\ & -A_{P1}(t_j)\,P[t_j-\tau_1(t_j)]W[t_j-\tau_1(t_j)]D[t_j-\tau_1(t_j)]\sin[\omega_{\text{ifL1}}t_j+s_1\phi_1(t_j)] \\ & +A_{P2}(t_j)\,P[t_j-\tau_2(t_j)]W[t_j-\tau_2(t_j)]D[t_j-\tau_2(t_j)]\cos[\omega_{\text{ifL2}}t_j+s_2\phi_2(t_j)] \\ & +n(t_j) \end{aligned} \tag{1}$$

where t_j is the sample time, y is the front end's output signal, A_C is the amplitude of L1 C/A carrier, A_{P1} is the amplitude of L1 P(Y) carrier, A_{P2} is the amplitude of L2 P(Y) carrier, *C* is C/A PRN code, *W* is the encrypted W PRN code, *P* is the known P PRN code, *D* is the 50 Hz navigation data bit stream, ϕ_1 is the carrier phase of L1, ϕ_2 is the carrier phase of L2, ω_{ifL1} is the intermediate value of the L1 carrier frequency, ω_{ifL2} is the intermediate value of the L2 carrier frequency, s_1 and s_2 are signs to reflect the possibility of phase reversial at the intermediate frequency (+1 for no phase reversial, -1 for a phase-reversial as in high-side mixing), τ_1 is the PRN code phase of L1, τ_2 is the PRN code phase of L2, and n is noise. The noise n is zero-mean discrete time Gaussian

(almost) white noise with a one-sided power spectral density of N_{01} near ω_{ifL1} and N_{02} near ω_{ifL2}. The coupling of L1 and L2 frequency bands in a single output is a feature of the multi-frequency direct RF sampling front end that has been used in this study [4]. It has been designed so that ω_{ifL1} and ω_{ifL2} are well separated. It is straight forward to adopt the present algorithm to a more conventional dual-frequency RF front end, which has separate outputs for the L1 and L2 frequency bands.

Equation (1) shows the fact that the P(Y) carrier on L1 has a 90 deg phase offset from the C/A carrier while the L1 P(Y) code has the same code phase as the C/A code. Therefore, the carrier phase and the code phase from C/A tracking can be used to deduce P(Y) carrier and code phase on L1. Decoded navigation data bits from L1 C/A tracking also provide a handover word. The time-of-week count in this handover word enables synchronization of a P code reconstruction with the received L1 P(Y) code.

B. Signal Amplitude and Phase Dynamics Model

The tracking algorithm uses a discrete-time dynamics model of the time evolution of the L2 signal's carrier and code phase and of the L1 and L2 P(Y) carrier amplitudes. This model includes 6 states $x_k = [x_p; x_\omega; x_\alpha; T; A_{P2}; A_{P1}]_k$ and takes the form

$$\begin{bmatrix} x_p \\ x_\omega \\ x_\alpha \end{bmatrix}_{k+1} = \begin{bmatrix} 1 & \Delta T_k & \frac{\Delta T_k^2}{2} \\ 0 & 1 & \Delta T_k \\ 0 & 0 & 1 \end{bmatrix} \begin{bmatrix} x_p \\ x_\omega \\ x_\alpha \end{bmatrix}_k - \begin{bmatrix} \Delta T_k \\ 0 \\ 0 \end{bmatrix} \omega_{NCOk} + \begin{bmatrix} 1 & 0 & 0 & 0 \\ 0 & 1 & 0 & 0 \\ 0 & 0 & 1 & 0 \end{bmatrix} w_{\phi k}$$

$$T_{k+1} = T_k + \frac{\omega_{L2}\Delta T_{nomk} - (w_{\phi k})_1}{\omega_{L2} + x_{\alpha k} + 0.5\Delta T_{nomk} x_{\alpha k}} + w_{Tk} \qquad (2)$$

$$A_{P2k+1} = A_{P2k} + w_{p2k}$$

$$A_{P1k+1} = A_{P1k} + w_{p1k}$$

where k is index of the W chip start/stop times, x_p is the carrier phase difference between the true L2 carrier and the receiver's L2 carrier numerically controlled oscillator (NCO), x_ω is the true L2 carrier Doppler shift, x_α is the rate of change of the L2 carrier Doppler shift, T is the true start/stop times of one W code chip and is a measure of the P(Y) code phase, ω_{NCO} is the receiver's L2 carrier NCO Doppler shift, $\Delta T_k = T_{NCO(k+1)} - T_{NCOk}$ is the accumulation interval, $\omega_{L2} = 1227.6 \times 10^6 \times 2\pi$ rad/sec is the nominal L2 carrier frequency, ΔT_{nomk} is the nominal period of the k-th W code chip. Equation (2) models carrier phase dynamics (the initial 3×1 vector equation), code phase dynamics (the 2nd equation), and carrier amplitude dynamics (the 3rd and 4th equations). The first 5 states apply to the P(Y) signal on L2, and the last dynamics equation is for the P(Y) amplitude on the L1 carrier. The 4×1 vector $w_{\phi k}$ and the scalar w_{Tk}, w_{p2k}, and w_{p1k} are discrete-time Gaussian white process noise. Suitable covariance matrices for these white noise processes are given in Ref. 5. The white-noise model for the carrier phase dynamics includes random walk acceleration of the line-of-sight (LOS) vector to the GPS satellites and the receiver clock's phase and frequency random walk. The white noise that drives the code phase dynamics equation represents code-carrier divergence due to ionospheric effects. The random-walk carrier amplitude models in the 3rd and 4th equations allow for dynamic amplitude variations due to ionospheric scintillation and other effects.

C. Carrier Phase Error and Code Phase Error Models

For purpose of this analysis, the carrier phase error is determined to be difference between the true carrier phase and the carrier phase of the receiver's carrier NCO, which is used to perform base-band mixing in preparation for the accumulation of correlations. Similarly, the code phase error is derived to be the difference between the true code phase and the code phase of the receiver's P-code NCO. These two phase errors can be expressed in terms of the estimated state. The average carrier phase error over one W chip accumulation interval is modeled as:

$$\Delta\phi_k = \begin{bmatrix} 1 & \frac{\Delta T_k}{2} & \frac{\Delta T_k^2}{6} \end{bmatrix} \begin{bmatrix} x_p \\ x_\omega \\ x_\alpha \end{bmatrix}_k - \frac{\Delta T_k}{2}\omega_{NCOk} + \begin{bmatrix} 0 & 0 & 0 & 1 \end{bmatrix} w_{\phi k} \qquad (3)$$

Similarly, the average code phase error over an accumulation interval is

$$\begin{aligned} \Delta\tau_k &= 0.5(T_{NCOk} + T_{NCOk+1}) - 0.5(T_k + T_{k+1}) \\ &= 0.5(T_{NCOk} + T_{NCOk+1}) - T_k - 0.5\frac{\omega_{L2}\Delta T_{nomk} - (w_{\phi k})_1}{\omega_{L2} + x_{\alpha k} + 0.5\Delta T_{nomk} x_{\alpha k}} \end{aligned} \qquad (4)$$

D. Measurement Model

The measurements used on the tracking algorithm are a quadrature W-bit accumulation on L1 and in-phase and quadrature W-bit accumulations on L2. For the L2 accumulations, prompt and early-minus-late versions are used, the latter to sense code phase. The resulting measurement vector is

$$y_{meask} = \begin{bmatrix} Q_{L1k} \\ I_{L2pk} \\ I_{L2emlk} \\ Q_{L2pk} \\ Q_{L2emlk} \end{bmatrix} \qquad (5)$$

where Q_{L1} is the quadrature accumulation on L1, I_{L2p} is the in-phase prompt accumulation on L2, I_{L2eml} is the in-phase early-minus-late accumulation on L2, Q_{L2p} is the quadrature in-phase prompt accumulation on L2, and Q_{L2eml} is the quadrature early-minus-late accumulation on L2. These L1 and L2 accumulations are calculated using the following equations, which mix the signals to base band and with the receiver's reconstructed P code before summing accumulation:

$$
\begin{aligned}
Q_{L1k} &= -\sum \left\{ y(t_j)\ \sin\left[\omega_{ifL1} t_j + s_1 \hat{\phi}_{L1}(t_j)\right] P(t_j - \hat{\tau}_{1k}) \right\} \\
I_{L2k}(\Delta) &= \sum \left\{ y(t_j) \cos\left[\omega_{if_{L2}} t_j + s_2 \phi_{L2NCO}(t_j)\right] P(t_j - \tau_{2NCOk} + \Delta) \right\} \\
Q_{L2k}(\Delta) &= -\sum \left\{ y(t_j) \sin\left[\omega_{if_{L2}} t_j + s_2 \phi_{L2NCO}(t_j)\right] P(t_j - \tau_{2NCOk} + \Delta) \right\} \\
I_{L2pk} &= I_{L2k}(0) \\
I_{L2emlk} &= I_{L2k}(\Delta_{eml}/2) - I_{L2k}(-\Delta_{eml}/2) \\
Q_{L2pk} &= Q_{L2k}(0) \\
Q_{L2emlk} &= Q_{L2k}(\Delta_{eml}/2) - Q_{L2k}(-\Delta_{eml}/2)
\end{aligned}
\tag{6}
$$

where $\hat{\phi}_{L1}$ is the estimated carrier phase of L1 from C/A code tracking, $\hat{\tau}_{1k}$ is the estimated code phase of L1 from C/A code tracking, ϕ_{L2NCO} is the receiver's reconstructed carrier phase of L2, and τ_{2NCOk} is the receiver's prompt P code start time for L2. The L2 P-code offset Δ yields in early accumulation if it is positive and a late accumulation if it is negative. The offset Δ_{eml} is the code delay of the late signal behind the early signal. The *k*-th accumulation is nominally one W chip in length. It starts at T_{NCOk} and ends at $T_{NCO(k+1)}$.

This summation of accumulations over each W chip is the hallmark of semi-codeless P(Y) tracking algorithm. They are called semi-codeless because they use the known P code even though they do not know the W chips. The mixing with P(Y) code replica and the carrier replica in eq. (6) leaves only the unknown W chips and noise on the signal (if all phase errors are zero). Summation over each W chip increases the SNR, which improves the accuracy of W bit estimation. The increased pre-detection SNR that mostly from summation over an entire W bit is what enables semi-codeless techniques to perform better than codeless techniques.

A model of measurement vector can be derived by using eqs. (1) and (6). It takes the form:

$$
\begin{aligned}
y_{\mathrm{mod}\,k} &= \frac{1}{2}\begin{bmatrix} A_{P1k} N_{1k} \\ A_{P2k} N_{2k} \cos(\Delta\phi_k) R_p(\Delta\tau_k) \\ A_{P2k} N_{2k} \cos(\Delta\phi_k) R_{eml}(\Delta\tau_k) \\ s_2 A_{P2k} N_{2k} \sin(\Delta\phi_k) R_p(\Delta\tau_k) \\ s_2 A_{P2k} N_{2k} \sin(\Delta\phi_k) R_{eml}(\Delta\tau_k) \end{bmatrix} W_k \\
&+ \begin{bmatrix} n_{QL1k} \\ n_{IL2pk} \\ n_{IL2emlk} \\ n_{QL2pk} \\ n_{QL2emlk} \end{bmatrix} = h(x_k) W_k + n_k
\end{aligned}
\tag{7}
$$

where N_{1k} and N_{2k} are the number of RF front end samples in the accumulation interval for L1 and L2, respectively, $\Delta\phi_k$ is the average carrier phase error over the accumulation interval, $\Delta\tau_k$ is the average code phase error over the accumulation interval, $R_p(\Delta\tau_k)$ is the normalized prompt autocorrelation function of the P PRN code, $R_{eml}(\Delta\tau_k)$ is the early-minus-late autocorrelation function of the P PRN code. The vector n_k is a zero-mean, uncorrelated Gaussian white-noise measurement error vector. The variances of its components are as follows: The variance of n_{QL1k} is $\sigma^2_{Q1k} = N_{01} N_{1k} / (4\Delta t_s)$. The components n_{IL2pk} and n_{QL2pk} both have variances $\sigma^2_{IQ2pk} = N_{02} N_{2k} / (4\Delta t_s)$ and the components $n_{IL2emlk}$ and $n_{QL2emlk}$ have variances $\sigma^2_{IQ2emlk} = 2\sigma^2_{IQ2pk}[1 - R_p(\Delta_{eml})]$. The quantity Δt_s is the RF front end sample period, $\Delta t_s = t_{j+1} - t_j$. Recall that the quantities N_{01} and N_{02} are the single-sided noise power spectral densities near the L1 and L2 intermediate carrier frequency. Note how eq. (7) effectively defines the vector function $h(x_k)$. The measurement model for Q_{L1} does not contain carrier or code phase errors because the estimated carrier phase error on L1 ($\Delta\hat{\phi}_1$) and the estimated code phase error on L1 ($\Delta\hat{\tau}_1$) are assumed to be zero due to accurate C/A tracking.

The model in eq. (7) is the function of $A_{P1k}, A_{P2k}, \Delta\phi_k, \Delta\tau_k$, and W_k. The quantities A_{P1k} and A_{P2k} are states to be estimated, and the quantities $\Delta\phi_k$ and $\Delta\tau_k$ are function of states to be estimated – review eqs. (3) and (4). The unknown W chip W_k in eq. (7) is not a state that is directly estimated by the EKF. The EKF effectively forms an optimal estimate of W_k along with a measure of its confidence in its estimate. It does this by using a ln(cosh()) term in the cost function that is minimized as a part of its estimation procedure.

IV. AN EXTENDED KALMAN-FILTER FOR P(Y) CODE AND CARRIER TRACKING ON L2

A. Cost Function of EKF

The EKF approximately solves a nonlinear weighted least-square problem by approximately determining the state vector $x_k = [x_p; x_\omega; x_\alpha; T; A_{P2}; A_{P1}]_k$ that minimizes the cost function:

$$J_k = \frac{1}{2}\left[\widetilde{R}_{xxk}(x_k - \widetilde{x}_k)\right]^T\left[\widetilde{R}_{xxk}(x_k - \widetilde{x}_k)\right] + \frac{1}{2}\left[R_{wwk}\, w_k\right]^T\left[R_{wwk}\, w_k\right] + J_{meask} \quad (8)$$

where $\widetilde{x}_k$ is an a priori estimate of x_k based on all previous accumulations up through time T_{NCOk}, $\widetilde{R}_{xxk}$ is the a priori estimation error square root information matrix, R_{wwk} is the a priori process noise square root information matrix, $w_k = [w_{\phi k}; w_{Tk}; w_{p2k}; w_{p1k}]$ is the process noise vector, and J_{meask} is the cost function term involving the new *k*-th accumulation measurement data for the time interval T_{NCOk} to $T_{NCO(k+1)}$. This form of the filter's measurement update cost function is used because it allows one to implement the filter and the smoother using square-root-information filter (SRIF), as in Ref. (5). SRIF methods provide increased numerical stability. SRIF techniques work with square root information matrices such as $\widetilde{R}_{xxk}$ and R_{wwk} instead of the usual estimation error covariance matrices of a standard Kalman filter. If *P* is covariance, then the associated square-root-information matrix is *R* where $P = R^{-1}(R^T)^{-1}$. J_{meask} is defined as:

$$\begin{aligned} J_{meask} &= \frac{1}{2}\left[y_{meask} - y_{\mathrm{mod}k}\right]^T R_{yyk}^T R_{yyk}\left[y_{meask} - y_{\mathrm{mod}k}\right] \\ &= \frac{1}{2}\left[y_{meask} - h(x_k)W_k\right]^T R_{yyk}^T R_{yyk}\left[y_{meask} - h(x_k)W_k\right] \\ &= \frac{1}{2}\, y_{meask}{}^T R_{yyk}^T R_{yyk} y_{meask} + \frac{1}{2}h(x_k)^T R_{yyk}^T R_{yyk} h(x_k) \\ &\quad - y_{meas}{}^T R_{yyk}^T R_{yyk} h(x_k) W_k \end{aligned} \quad (9)$$

where R_{yyk} is a measurement error square root information matrix and is calculated from the measurement error covariance P_{yyk}:

$P_{yyk} = E\{n_k n_k\}^T = (R_{yyk}^T R_{yyk})^{-1}$, where

$$R_{yyk} = diag\left[\frac{1}{\sigma_{Q1k}}, \frac{1}{\sigma_{IQ2pk}}, \frac{1}{\sigma_{IQ2emlk}}, \frac{1}{\sigma_{IQ2pk}}, \frac{1}{\sigma_{IQ2emlk}}\right].$$

The last term on the 4th line at eq. (9) takes the form $-y_o W_k$, where $y_o = y_{meas}{}^T R_{yy}^T R_{yy} h(x_k)$. In effect, it gets used to estimate the unknown W bit. "Hard" W-bit estimation uses the approximation $W_k = sign[y_o]$ with $x_k = \widetilde{x}_k$ in the formula for y_o. The last term of J_{meask} then becomes $-abs[y_o]$. "Soft" W-bit estimation uses $W_k = 0.5[y_o]$, and the last term of J_{meask} becomes $-0.5y_o^2$. "Hard" W-bit estimation can be too decisive and can lead to frequent mis-identification if the W-bit SNR is small for an accumulation interval of about 2 μsec. "Soft" W-bit estimation, however, is more flexible because it weights its W-bit sign decision more heavily when the signal is strong and less heavily when the signal is weak and thus minimizes the effects of mis-identified W-bit signs.

The cost function in eq. (8) is the negative log of the a posteriori probability density function. The original probability density function is $P(x_k, w_k) = C\exp[-J_k]$ where *C* is constant. If one assumes that the probability of the W-bit being either +1 or –1 is equal, then the W-bit can be integrated out to yield a probability density function for *x* alone:

$$P(x_k) = C\left\{\frac{1}{2}\exp[-J_k\,|_{W=1}] + \frac{1}{2}\exp[-J_k\,|_{W=-1}]\right\}.$$

A new a posteriori cost function can then be written:

$$\begin{aligned} J_k &= -\ln[P(x_k)] = \frac{1}{2}\left[\widetilde{R}_{xxk}(x_k - \widetilde{x}_k)\right]^T\left[\widetilde{R}_{xx}(x_k - \widetilde{x}_k)\right] \\ &\quad + \frac{1}{2}\left[R_{wwk}w_k\right]^T\left[R_{wwk}w_k\right] \\ &\quad + \frac{1}{2}\, y_{meask}{}^T R_{yyk}^T R_{yyk} y_{meask} + \frac{1}{2}h(x_k)^T R_{yyk}^T R_{yyk} h(x_k) \\ &\quad - \ln\left[\cosh(y_{meask}{}^T R_{yyk}^T R_{yyk} h(x_k))\right] \end{aligned} \quad (10)$$

Unlike eq. (9), eq. (10) do not include the unknown W-bit explicitly. The ln[cosh(y_o)] term in eq. (10) effectively decides about the W-bit based on y_o, which is a function of the amplitude of the P(Y) signal on L1 and L2 and a function of the L1 carrier phase error. ln[cosh(y_o)]≅[abs(y_o)-ln2] when abs(y_o) is big, which corresponds to "hard" W-bit estimation. The ln[cosh(y_o)] term performs "soft" W-bit estimation when abs(y_o) is small because ln[cosh(y_o)] can be approximated as $0.5y_o^2$ in this case. Therefore, the ln[cosh(y_o)] term in the eq. (10) cost function optimally decides the W bit either by "hard" W-bit estimation, "soft" W-bit estimation, or a combination thereof, depending on the signal strength.

Another important fact about the ln[cosh(y_o)] term is that it is approximately a quadratic function ($0.5y_o^2$) when the signal is weak. This quadratic function of y_o includes squaring of the quadrature accumulation of L1, squaring

of the in-phase and quadrature accumulations of L2, and cross-correlation of L1 accumulations with L2 accumulations. Therefore, optimal L2 P(Y) tracking that uses a cost function involving ln[cosh(y_o)] term effectively implements a seamless transition between various semi-codelss W-bit estimation techniques; squaring, cross-correlation, soft-W bit decision, etc. The question of which terms dominate or of whether various terms have relatively equal importance is determined by their relative amplitudes. These relative amplitudes are a function of the A_{p1} and A_{p2} amplitude estimates. This is why it is so important to include estimation of these two signal amplitudes as part of the tracking algorithms.

B. Solution of the EKF Measurement Update and State Estimate Propagation

Finding the solution x_k that minimizes eq. (10) corresponds to the usual measurement update process of an EKF. This process is carried out for each W-chip interval. The minimization of eq. (10) uses one iteration of Newton's method. It minimizes a quadratic approximation of eq. (10). The quadratic approximation is calculated about the a priori estimate ($\tilde{x}_k, \tilde{w}_k = 0$). If the solution to the quadratic approximation of the measurement update problem is ($\delta x_k, \delta w_k$), then the a posteriori estimates are $\hat{x}_k = \tilde{x}_k + \delta x_k$ and $\hat{w}_k = \delta w_k$. The a posteriori estimation error square root information matrix, $\hat{R}_{xxk}$, is calculated from the Hessian matrix of the cost function eq. (10) [6]. To complete the recursive application of the EKF technique, $\tilde{x}_{k+1}$ and $\tilde{R}_{xx(k+1)}$ are calculated from $\hat{x}_k$ and $\hat{R}_{xxk}$ using the dynamics model in eq. (2). This is the propagation stage of the EKF. Propagation of the state is accomplished by iterating eq. (2) once with $\hat{x}_k$ and $\hat{w}_k$ input on the right-hand side and $\tilde{x}_{k+1}$ output on the left-hand side. $\tilde{R}_{xx(k+1)}$ is calculated from a QR factorization that includes a linearized version of the dynamics model in eq. (2) and the Hessian matrix of the cost function in eq. (10) [5]. Additional details about the implication of this SRIF can be found in Refs. (5) and (6).

C. Implementation of a PLL and a DLL

The tracking algorithm needs to implement a PLL and a DLL in order to create the carrier and code reconstruction that are used to compute accumulation in eq. (6). The receiver's reconstructed code and carrier phases are defined in terms of NCO W-chip start/stop times, $T_{NCO(k)}$, and carrier Doppler shifts. They can be calculated based on the estimated Kalman filter state by using the following feedback control law [7]:

$$T_{NCO\,(k+3)} = \tilde{T}_{k+1} + \frac{\omega_{L2}\Delta \mathrm{T}_{\mathrm{nom(k+1)}}}{\omega_{L2} + \tilde{x}_{\omega(k+1)} + 0.5\Delta T_{k+1}\tilde{x}_{\alpha(k+1)}} + \frac{\omega_{L2}\Delta \mathrm{T}_{\mathrm{nom(k+2)}}}{\omega_{L2} + \tilde{x}_{\omega(k+1)} + (\Delta \mathrm{T}_{k+1} + 0.5\Delta \mathrm{T}_{k+2})\tilde{x}_{\alpha(k+1)}} \tag{11}$$

$$\omega_{\mathrm{NCO(k+2)}} = \Big\{(1-\alpha)^2\tilde{x}_{p(k+1)} + \big[(1-2\alpha)\Delta T_{k+1} + \Delta T_{k+2}\big]\tilde{x}_{\omega(k+1)} + 0.5\big[-2\alpha\Delta T_{k+1}^2 + (\Delta T_{k+1} + \Delta T_{k+2})^2\big]\tilde{x}_{\alpha(k+1)} - (1-2\alpha)\omega_{NCO(k+1)}\Delta T_{k+1}\Big\}/\,\Delta T_{k+2} \tag{12}$$

where α is a tuning parameter in the range of $0 \le \alpha < 1$. α should be near one for weak signal tracking to avoid jerky response of ω_{NCO} and achieve slow convergence of ω_{NCO}. $\omega_{\mathrm{NCO(k+2)}}$ applies during the time span $T_{NCO(k+2)}$ to $T_{NCO(k+3)}$.

V. EXPERIMENTAL TEST RESULTS

A. Dual-frequency RF Front End Development and Data Collection

A prototype dual-frequency RF front end has been developed using the technique of direct RF sampling with intentional aliasing [4]. Directly sampled RF data with a carefully chosen sampling frequency intentionally aliases the L1 and L2 bands down to non-overlapping intermediate frequency bands below half the sampling frequency. Test data for this paper's algorithm has been collected using this front end.

Data was collected on Feb. 27, 2003 with the sampling frequency 99.23 MHz. The intermediate carrier frequencies corresponding to this sampling frequency are ω_{ifL1} = $12.26\times10^6\times2\pi$ rad/sec and ω_{ifL2} = $36.84\times10^6\times2\pi$ rad/sec. There is a phase reversal on the aliased L1 signal (s_1=-1 in eq. (1)), and there is no phase reversal for L2 (s_2=+1). The signal from PRN No. 24 has been acquired and tracked. Its C/A code has a C/N_0 of 54.6 dB Hz. The L1 and L2 noise spectral densities at the output of the RF front end are $N_{01} = -73.3\,\mathrm{dB\,Hz^{-1}}$ and $N_{02} = -70.2\,\mathrm{dB\,Hz^{-1}}$. These are needed for calculating σ_{Q1k}, σ_{IQ2pk}, and $\sigma_{IQ2emlk}$, which are needed to construct the R_{yyk} matrix of eq. (9).

B. EKF based P(Y) Tracking Results

Figure 1 shows time histories of the three L2 carrier phase states estimates $[x_p; x_\omega; x_\alpha]$. The top plot, $x_p(t)$, is the

carrier phase difference between the true L2 carrier and the receiver NCO's L2 carrier. It converges quickly to a mean value of zero. The middle plot shows $x_\omega(t)$, the estimated L2 carrier Doppler shift, and the bottom plot shows $x_\alpha(t)$, the estimated rate of change of the L2 carrier Doppler shift. The EKF's computed estimation error standard deviations, which come from the $\hat{R}_{xxk}$ matrix are small: 0.67° for x_p, 0.027 Hz for x_ω, 0.07 Hz/sec for x_α.

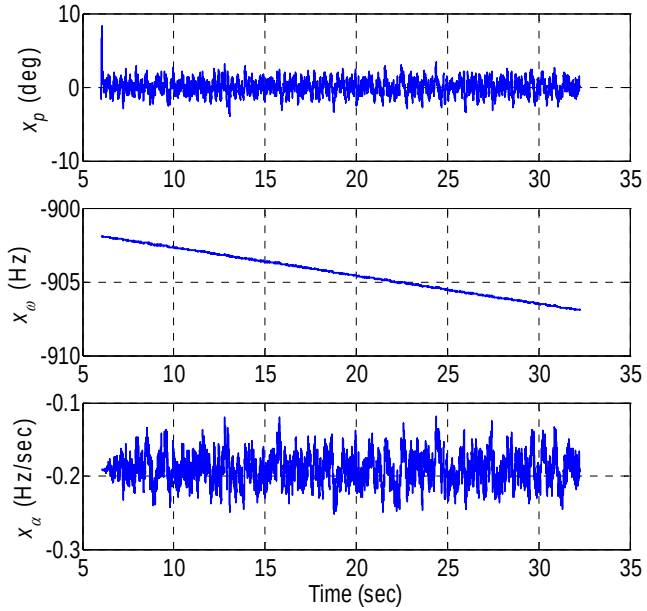

Fig. 1. Time histories of the EKF's estimated L2 carrier phase states $[x_p; x_\omega; x_\alpha]$

Figure 2 plots the EKF's estimated P(Y) carrier amplitude time histories for L1 and L2. The estimated average amplitudes are $A_{p1} = 0.15$ and $A_{p2} = 0.18$, and the EKF's computed amplitude error standard deviation are on the order of 10^{-4} for both L1 and L2. The estimated L2 signal strength is 1.6 dB stronger than the estimated L1 strength, $10\log_{10}[(0.18/0.15)^2] = 1.6$ dB. This contradicts the known fact that P(Y) on L2 is normally 3 dB weaker than P(Y) on L1 [8]. Most of this discrepancy is caused by the fact that the gain of the L2 path in the RF front end is 3 dB higher than the gain in the L1 path [4]. Therefore, the L2 P(Y) power estimate is actually about 1.4 dB weaker than L1 P(Y) power estimate. The remaining slight discrepancy of the power ratio from its nominal 3 dB value may be due to different L1 and L2 bandwidths of the multi-band bandpass filter in the dual-frequency RF front end, or it may be due to off-nominal operation of PRN No. 24 [4].

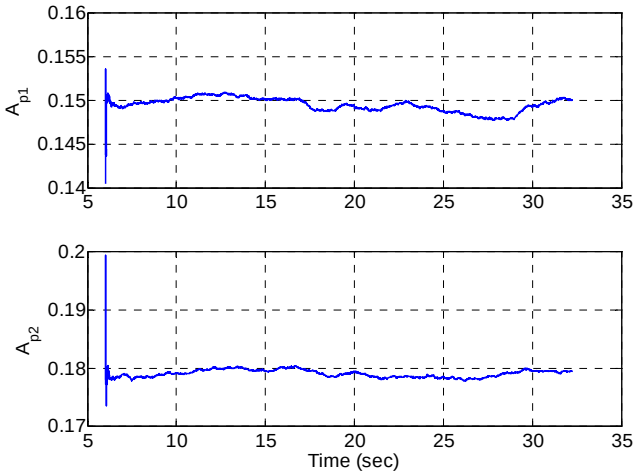

Fig. 2. The estimated P(Y) carrier amplitude time histories for L1 (top plot) and L2 (bottom plot).

Figure 3 compares two estimates of the LOS velocity. One comes from the L1 C/A tracking loop and the other comes from this paper's semi-codeless tracking. This comparison is used to determine whether the Doppler shift from L2 tracking agrees with the Doppler shift from L1 tracking. One cannot directly compare the Doppler shifts of the two carriers due to their different carrier frequencies. L2 tracking starts around 6 second. The estimated LOS velocity from L2 P(Y) tracking shows good agreement with the estimated LOS velocity from L1 C/A tracking.

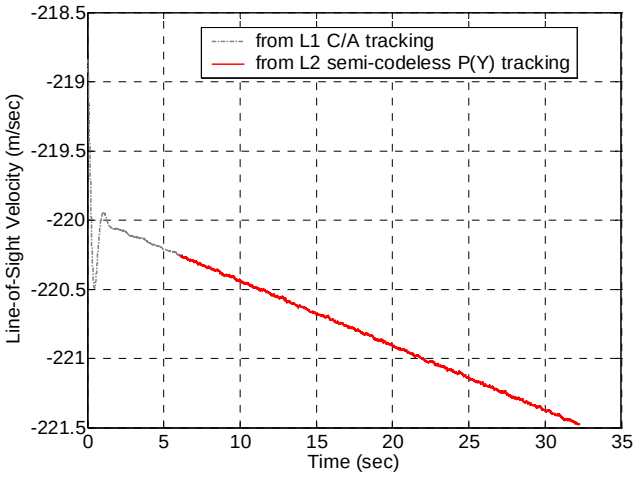

Fig. 3. A comparison of the LOS velocity estimate from the L1 C/A carrier tracking loop and that of the L2 P(Y) semi-codeless tracking algorithm.

Figure 4 shows time histories of the code delay of P(Y) on L2 with respect to P(Y) on L1. The average code delay of L2 vs. L1 is about 0.228 P code chips. This delay

corresponds to 22.3 nsec or 63.8 TEC units, which is reasonable.

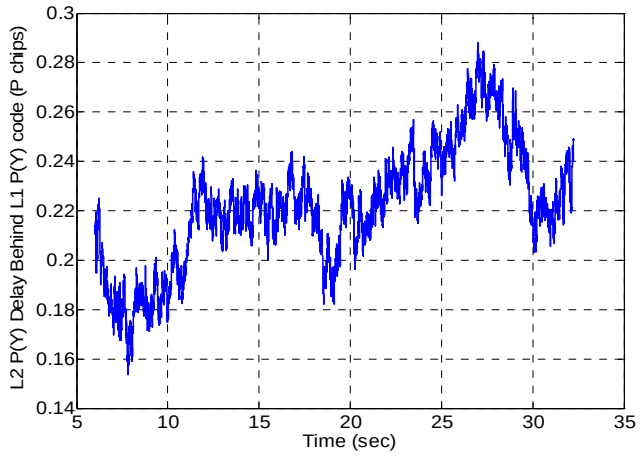

Fig. 4. Time histories of the code delay of P(Y) on L2 with respect to P(Y) on L1.

C. Tuning of the EKF

The proper tuning of the EKF is important for good semi-codeless weak signal tracking performance. The tuning can be modified by varying the process noise square-root-information matrix R_{wwk} and the measurement noise square-root information matrix R_{yyk}. Since the measurement noise square-root information matrix is likely to be reasonable based on N_{01} and N_{02}, one normally adjusts R_{wwk} to tune the EKF. If one increases the process noise intensity, the EKF has a higher bandwidth and converges more rapidly but with increased estimation error variance. A decrease of the process noise intensity reduces bandwidth, slows convergence of filter, and decreases the estimation error variance. Of course, the proper tuning depends on the needed bandwidth which is a function of the expected signal dynamics bandwidth. One must be careful not to use too high-tuning of the L2 tracking algorithm, i.e. one must not use R_{wwk} values that are too small. Otherwise, the P(Y) semi-codeless tracking algorithm responds too quickly to a possibly mis-identified W-bit at each W bit interval. A slow (i.e. low bandwidth) tuning with less than few Hz bandwidth is reasonable for the current approach. A slow tuning allows the filter to respond slowly to possibly mis-identified W-bits, and the estimation becomes more reasonable because the filter averages over longer data intervals which will have a predominance of correctly decided W-bits.

A slow tuning with about a 1 Hz bandwidth has been used to generate results for Figs. 1-4. R_{wwk} depends on random walk intensities and ΔT_k. R_{wwk} is a 7×7 matrix with a non-zero upper left-hand 4×4 block, a non-zero lower right-hand 3×3 diagonal matrix, and zeros elsewhere. The upper left-hand 4×4 block of R_{wwk} depends on three intensity parameters, as defined in eq. (8) of Ref. 6. The LOS acceleration random walk intensity, q_{LOS} = 0.2 rad^2/sec^5, the receiver clock frequency random walk intensity, $S_g = 3\times10^{-21}$ sec^{-1}, and the receiver clock phase random walk intensity, $S_f = 1\times10^{-20}$ sec, have been used to generate Figs. 1-4. The lower right-hand 3×3 diagonal block is a function of the random walk intensities for the code phase, and the two carrier amplitudes:

$$(R_{wwk})_{\mathrm{lower3\times3}} = diag\left[\frac{1}{\sqrt{\Delta T_k q_T}}, \frac{1}{\sqrt{\Delta T_k q_{Ap2}}}, \frac{1}{\sqrt{\Delta T_k q_{Ap1}}}\right],$$

where the values $q_T = 1\times10^{-20}$ sec^2/sec, and $q_{Ap2} = 1.6\times10^{-7}$ (RF-front end units^2/sec), and $q_{Ap1} = 9.9\times10^{-8}$ (RF-front end units^2/sec) have been used. Also, the DLL tuning value α = 0.9999 has been used for these cases.

VI. CONCLUSIONS AND PLANNED FUTURE WORK

An EKF-based semi-codeless optimal P(Y) tracking algorithm has been developed to be used for weak dual-frequency GPS signals. This optimal algorithm effectively implements seamless transitions between various estimation techniques for the unknown W encryption bit, such as squaring, cross-correlation, soft W-bit estimation, etc. The algorithm has been successfully tested with signals from a dual-frequency RF front end under normal terrestrial signal strength conditions. Although the current algorithm has not yet been tested on weak signals, it is expected to perform at least as well as previously published semi-codeless techniques such as soft-bit decision Z-tracking and the MAP method because of its complete implementation of a posteriori estimation techniques.

Future efforts to improve and verify the performance of the current algorithm will include three aspects. First, the present algorithm will be tested using weak signals. Weak signals will be simulated, and real data will be collected under scintillating conditions. The simulated scintillation data will be semi-experimental in that it will consist of actual tracking data from a dual-frequency RF front end, but with dynamic attenuation of the signal in order to simulate one of the two principal effects that occurs during strong ionospheric scintillations. Second, an optimal smoother will be developed to allow tracking of the weakest possible signals. A smoother uses past, current, and future information to find the best estimate at the current time. The smoother will give better estimates than the EKF, but will be applicable only for off-line processing. Third, the weak signal C/N$_0$ thresholds will be

found above which the Kalman-filter algorithm and the smoother algorithm can still track without losing the lock.

ACKNOWLDEGEMENTS

This work has been supported in part by the NASA office of Space Science through grant No. NAG5-12211. David Sibeck is the grant monitor.

REFERENCES

1. Woo, K.T., "Optimum Semicodeless Carrier-Phase Tracking of L2," *Navigation*, 47(2), 2000, pp. 82-99.

2. Lorenz, R.G., Helkey, R.J., and Abadi, K.K., "Global Positioning System Receiver Digital Processing Technique," U.S. Patent No. 5,134,407, July 1992.

3. Woo, R.K.T., Quan, J.O., and Cheng, U., "System and Method for Demodulating Global Positioning System Signals," U.S. Patent No. 6,125,135, Sept. 2000.

4. Psiaki, M.L., Powell, S.P, Jung, H, and Kintner, P.M. Jr., "Design and Practical Implementation of Multi-Frequency RF Front Ends Using Direct RF Sampling," *Proceedings of the ION GPS/GNSS 2003*, Sept. 9-12, 2003, Portland, OR.

5. Bierman, G.J., *Factorization Methods for Discrete Sequential Estimation*, Academic Press, (New York, 1977), pp. 69-76, 115-122, 214-217.

6. Psiaki, M.L., and Jung, H., "Extended Kalman Filter Methods for Tracking Weak GPS Signals," *Proceedings of the ION GPS 2002*, Sept. 24-27, 2002, Portland, OR. pp. 2539-2553.

7. Psiaki, M.L., "Smoother-Based GPS Signal Tracking in a Software Receiver." *Proceedings of the ION GPS 2001*, Sept. 11-14, 2001, Salt Lake City, UT, pp. 2900-2913.

8. Spilker, J.J., Jr., "GPS Signal Structure and Theoretical Performance," in *Global Positioning System: Theory and Applications, Vol. I*, Parkinson, B.W., and Spilker, J.J., Jr., eds., American Institute of Aeronautics and Astronautics, (Washington, 1996), pp. 57-119.